An omnidirectional electromagnetic absorber made of metamaterials

2010 New J. Phys. 12 063006

(http://iopscience.iop.org/1367-2630/12/6/063006)

New Journal of Physics
The open-access journal for physics

An omnidirectional electromagnetic absorber made of metamaterials

Qiang Cheng, Tie Jun Cui[1], Wei Xiang Jiang and Ben Geng Cai
State Key Laboratory of Millimeter Waves, Department of Radio Engineering, Southeast University, Nanjing 210096, People's Republic of China
E-mail: tjcui@seu.edu.cn

New Journal of Physics **12** (2010) 063006 (10pp)
Received 24 January 2010
Published 3 June 2010
Online at http://www.njp.org/
doi:10.1088/1367-2630/12/6/063006

Abstract. In a recent theoretical work by Narimanov and Kildishev (2009 *Appl. Phys. Lett.* **95** 041106) an optical omnidirectional light absorber based on metamaterials was proposed, in which theoretical analysis and numerical simulations showed that all optical waves hitting the absorber are trapped and absorbed. Here we report the first experimental demonstration of an omnidirectional electromagnetic absorber in the microwave frequency. The proposed device is composed of non-resonant and resonant metamaterial structures, which can trap and absorb electromagnetic waves coming from all directions spirally inwards without any reflections due to the local control of electromagnetic fields. It is shown that the absorption rate can reach 99 per cent in the microwave frequency. The all-directional full absorption property makes the device behave like an 'electromagnetic black body', and the wave trapping and absorbing properties simulate, to some extent, an 'electromagnetic black hole.' We expect that such a device could be used as a thermal emitting source and to harvest electromagnetic waves.

[1] Author to whom any correspondence should be addressed.

Contents

1. Introduction

In the past ten years research in metamaterials has attracted great interest in the scientific community. The experimental and theoretical advances in artificial metamaterials have offered scientists potent ways of tailoring the properties of electromagnetic waves in curvilinear space. Metamaterials have manifested several exciting effects and devices, such as negative refraction, electromagnetic invisibility cloaks, super-resolution imaging, electromagnetic concentrators and light trapping [1]–[17], in which the required constitutive parameters could be fulfilled by periodic/non-periodic arrays of electric or magnetic resonant/non-resonant particles. Current technologies for designing and fabricating metamaterials have enabled realization of such functional devices with unusual electromagnetic properties.

In this work, we realize an omnidirectional electromagnetic absorber in microwave frequencies, based on the theoretical prediction using non-magnetic metamaterials [16], which acts like an effective microwave 'black body' and absorbs incident waves from all directions efficiently. We designed and fabricated the omnidirectional electromagnetic absorbing device using non-resonant and resonant metamaterial structures, and measured internal electric fields using a planar-waveguide near-field scanning apparatus. Experimental results agree well with the full-wave numerical simulations, which show obvious phenomena of microwave bending and trapping spirally into the device without coming back. The device can absorb electromagnetic waves coming from all directions efficiently with an absorption rate of 99% in the microwave frequency, which could find wide applications in thermal emitting and microwave harvesting.

2. Analysis

In analytical mechanics, the motion of any particle can be described by Hamilton equations

$$\frac{\mathrm{d}}{\mathrm{d}t}p(t) = -\frac{\partial \mathcal{H}}{\partial q}, \qquad \frac{\mathrm{d}}{\mathrm{d}t}q(t) = \frac{\partial \mathcal{H}}{\partial p}, \tag{1}$$

in which p is the generalized momentum, q is the generalized coordinate and $\mathcal{H}$ is the Hamiltonian. The Hamiltonian represents the energy of the system, which is usually the sum of kinetic and potential energy, denoted by T and V, respectively, as $\mathcal{H} = T + V$, $T = p^2/(2m)$, $V = V(q)$, in which m is the mass of particle. All these could be deduced from the Hamilton principle.

In geometrical optics, similar to the Hamilton principle, the Fermat principle governs the propagation of light or electromagnetic waves. Considering that the eikonal function $S_t(r, \theta)$ in

a two-dimensional (2D) cylindrical coordinate is expanded in series $S_t(r,\theta) = S(r,\theta) - \omega t$ as a Hamilton–Jacobi equation, we could get the Hamiltonian in optics as [18]

$$\mathcal{H} = \frac{\omega^2}{2\mu_0} = \frac{{p_r}^2}{2\epsilon(r)} + \frac{p_\theta^2}{2r^2\epsilon(r)}, \tag{2}$$

in which $p_r = \partial S/\partial r$ and $p_\theta = \partial S/\partial\theta$ are the radial and angular momenta in the cylindrical coordinate, ω is the radian frequency, μ_0 is the magnetic permeability in free space and $\epsilon(r)$ is the electric permittivity in the isotropic non-magnetic medium. Since the frequency is invariant in a time-harmonic system, the above equation shows an energy conservation in mechanics. From the Hamilton equation, the trajectory of geometrical optics looks like a unit particle in a central potential that is given by [3]: $V_{\text{eff}}(r) = \omega^2 c^2[\epsilon_\text{b} - \epsilon(r)]/2$, in which ϵ_b is the background permittivity and c is the light speed. The inhomogeneous electric permittivity is chosen as

$$\epsilon(r) = \begin{cases} \epsilon_\text{b}, & r > R, \\ \epsilon_\text{s}(r) = \epsilon_\text{b}(R/r)^2, & R_\text{c} \leqslant r \leqslant R, \\ \epsilon_\text{c} + i\gamma, & r < R_\text{c}. \end{cases} \tag{3}$$

The above permittivity distribution describes a layered dielectric cylinder, which includes a lossy circular inner core and a lossless circular shell with radially varied permittivity, as shown in figure 1(a). Here, R_c and R stand for the radii of the inner core and the outer shell of the cylinder, while ϵ_b and ϵ_c represent the dielectric constants of the background medium and the lossy material inside the core. The radius of the core is closely related to the ratio of two dielectric constants: $R_\text{c} = R\sqrt{\epsilon_\text{b}/\epsilon_\text{c}}$. Under the ray approximation, it has been proved that the light or electromagnetic waves hitting the cylinder will bend spirally in the shell region, and be trapped and absorbed by the lossy core, as illustrated in figure 1(a). It is also shown that the scattering cross-section per unit length of the cylinder is nearly zero, which is independent of the polarization state of incident waves [16]. Hence the dielectric cylinder is a perfectly omnidirectional absorber, behaving like an 'electromagnetic black body' or an 'electromagnetic black hole' to some extent, which could absorb nearly all light or electromagnetic waves hitting it from every direction.

3. Results and discussions

In this section, we validate the electromagnetic omnidirectional absorber through numerical simulations and experiments in microwave frequency. From equation (3), the permittivity distribution of the absorber's outer shell ($R_\text{c} < r < R$) varies gradually from the inner core to the background medium. Hence the outer shell can be realized by gradient refraction index metamaterials, which have been used in the design of several new concept devices such as the invisibility [5] and ground-plane cloaks [7, 8].

A number of non-resonant metallic structures can be utilized as the basic element of gradient refraction index metamaterials, such as the circular ring, I-shaped structure, and Jerusalem cross. The dimensions of unit geometries can be adjusted to meet the demand of refraction indices at specific positions, to achieve the gradient distribution. In non-resonant metamaterials, the resonant frequencies of unit geometries are much higher than the operating frequency, and the dispersion curves for effective permittivity and permeability change slowly in a broad band. Considering the anisotropy of most metamaterial units, the electromagnetic constitutive parameters for the absorber are adjusted for the transverse-electric (TE) polarization

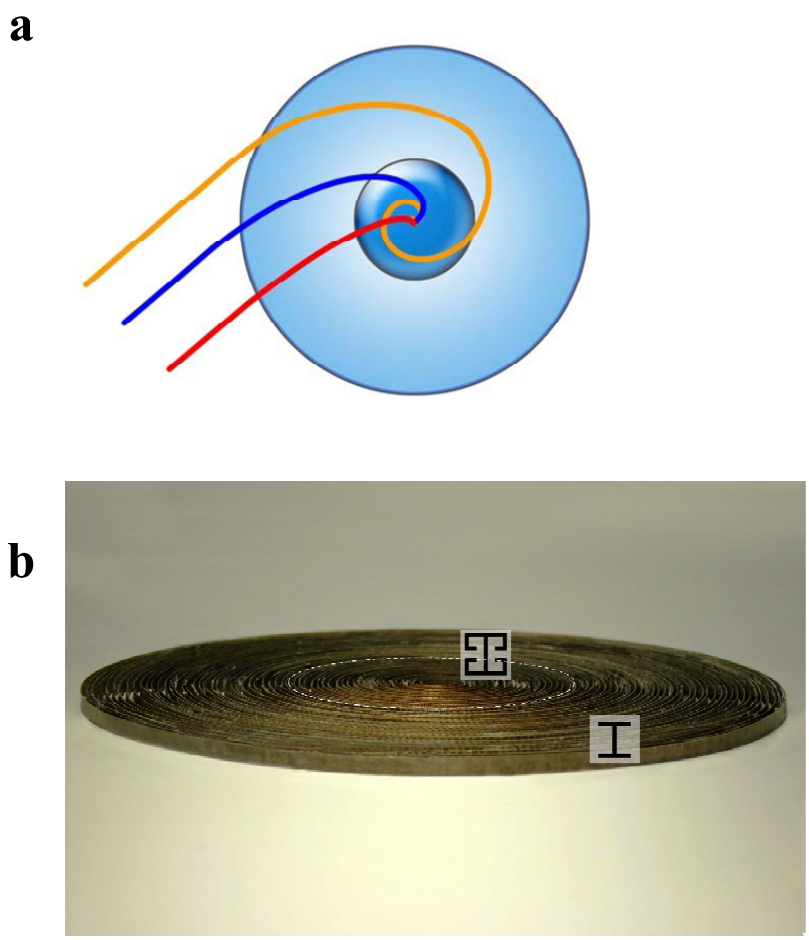

Figure 1. (a) A model of an electromagnetic omnidirectional absorber composed of a gradient-index metamaterial shell and a lossy dielectric core. (b) Photograph of the fabricated artificial omnidirectional absorbing device based on metamaterials, which is composed of 60 concentric layers, with ELC structures in the core layers and I-shaped structures in the shell layers.

in the cylindrical coordinate as $\epsilon_z = \epsilon(r)$, $\mu_\phi = 1$ and $\mu_r = 1$. In our design, we choose the non-resonant I-shaped structure [12] as the basic unit for the outer shell of the omnidirectional absorbing device, and the electric-field-coupled (ELC) resonator [14] as the basic unit for the inner core, which has large permittivity and large loss tangent simultaneously near the resonant frequency.

The photograph of the fabricated omnidirectional absorbing device is shown in figure 1(b), in which the I-shaped unit cell and ELC resonator are illustrated in figures 2(a) and (b), respectively. The device is placed in the air; hence the permittivity of the background medium is simply $\epsilon_b = 1$. In order to better demonstrate the absorption effect, a relatively high microwave frequency ($f = 18$ GHz) is selected in simulations and experiments. The sizes of both the I-shaped unit cell and the ELC resonator are set as 1.8 mm, nearly 1/10 free-space wavelength. The whole omnidirectional absorber is composed of 60 concentric layers, and each layer is a thin printed circuit board (F4B, $\epsilon = 2.65 + i0.001$) etched with a number of sub-wavelength

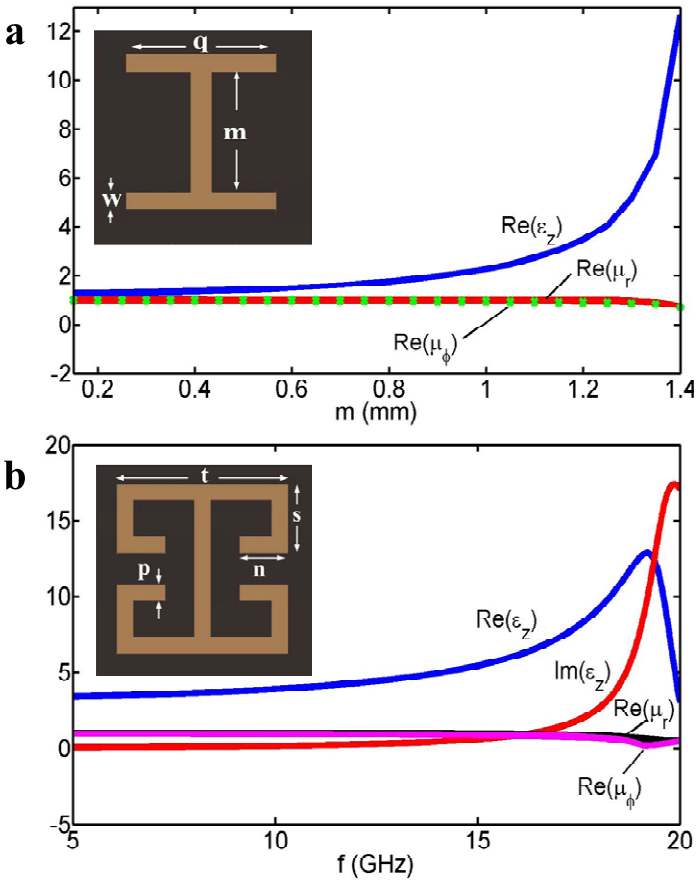

Figure 2. Effective medium parameters for unit cells of the artificial omnidirectional absorbing device. (a) The relation between the effective permittivity (real part of ϵ_z) and permeability (real parts of μ_r and μ_ϕ) and the geometry dimension m for the I-shaped unit. The inset shows the sketch of the I-shaped unit, with $w = 0.15$ mm and $q = 1.1$ m. (b) The effective permittivity (real and imaginary parts of ϵ_z) and permeability (real parts of μ_r and μ_ϕ) versus the frequency for the ELC resonator. The inset shows the sketch of the ELC unit, where $t = 1.6$ mm, $g = 0.3$ mm, $p = 0.15$ mm, and $s = 0.65$ mm.

unit structures. From equation (3), the permittivity changes radially in the shell of the absorber; hence the unit cells are identical in each layer but have different sizes in adjacent layers. Since the permittivity is a constant in the lossy core, the ELC resonators are identical in the whole region.

Figure 2 demonstrates the effective medium parameters of the I-shaped and ELC units for the designed device. The full-wave numerical tool (Microwave Studio, CST2006b) is used to simulate the electromagnetic properties. Following the standard retrieval procedure [19], the effective permittivity and permeability are obtained from the scattering parameters with the change of geometry dimensions. To determine the relation between geometry and medium parameters, an interpolation algorithm has been developed to generate the final layout according to the permittivity distribution required by the omnidirectional absorber. From figure 2(a), by changing the height of the I-shaped unit, the real part of permittivity Re(ϵ_z) ranges from 1.27

to 12.64 at 18 GHz, while the permeability components, $\mathrm{Re}(\mu_r)$ and $\mathrm{Re}(\mu_\phi)$, are always close to unity. The imaginary parts of permittivity and permeability for the I-shaped unit, not shown here, are small enough to be neglected in the design. From figure 2(b), the operating frequency is close to the resonant frequency of the ELC structure, which results in a very lossy permittivity $\epsilon_z = 9.20 + \mathrm{i}2.65$ and the permeability components $\mu_r = 0.68 - \mathrm{i}0.01$ and $\mu_\phi = 0.84 - \mathrm{i}0.14$ at 18 GHz.

In our design, the space between adjacent layers is 1.8 mm; hence the radii of the absorber and the lossy core are determined immediately as $R = 108$ mm and $R_c = 36$ mm. There are in total 40 layers of I-shaped structures and 20 layers of ELC structures. In order to fix the 60 layers with different radii together, a 0.8-mm-thick styrofoam board has been used with 60 concentric circular slots carved by the LPKF milling machine (LKPF s100). Each layer has three unit cells in the vertical direction, and hence the height of the absorber is 5.4 mm. To investigate the interactions between the fabricated absorber and incident TE-polarized electromagnetic waves, a parallel-plate waveguide near-field scanning system is used to map the field distributions near the absorber at 18 GHz. A similar apparatus is discussed in [20]. The separation between two plates is set as 6.5 mm, which is larger than the height of the device to avoid the unnecessary dragging during measurements. The cutoff frequency of the waveguide system for the dominant TEM mode is 23 GHz. The bottom plate is mounted on a step motor that can translate in two dimensions. A monopole probe is fixed inside the waveguide as the feeding source, and a corner reflector is placed on the back of source to produce the desired narrow beam. Four detection probes are placed on the top plate to measure the field distributions on a plane above the absorber under test, and each probe can scan a region of 200 mm × 200 mm independently. Hence the total scanning region is 400 mm × 400 mm with a step resolution of 0.5 mm. All probes are connected to a microwave switch that controls the measurement sequence after each movement of the step motors below the bottom plate. The two ports of a vector network analyzer (Agilent PNA-L N5230C) are connected to the feeding probe and the microwave switch, respectively, via cables. Then the measurement data are sent to the controlling computer for post processing.

To demonstrate the performance of the omnidirectional absorbing device in the microwave frequency, we first consider the case of Gaussian-beam incidence. Figures 3(a) and (b) illustrate the distributions of simulated electric fields $|E_z|$ at 18 GHz when a Gaussian beam is incident on the device on-center and off-center, respectively. We note that all on-center rays are directly attracted by the device without reflections, and nearly all off-center rays bend in the shell region spirally and are trapped by the core. To evaluate the absorption of the Gaussian beam by the device, we define an absorbing rate from the Poynting theorem as

$$\eta = P_{\mathrm{absorb}}/P_{\mathrm{in}}, \quad P_{\mathrm{absorb}} = -\tfrac{1}{2}\mathrm{Re}\left(\oint_s \vec{E} \times \vec{H}^* \cdot \mathrm{d}\vec{S}\right), \tag{4}$$

in which P_{absorb} is the net power entering the device surface and P_{in} is the incident power. Under the on-center and off-center incidences shown in figures 3(a) and (b), the absorbing rates are calculated as 99.94 and 98.72%, respectively. Clearly, nearly all incident powers are absorbed, and the device behaves like an 'electromagnetic black body'.

In experiments at microwave frequencies, however, it is difficult to generate the Gaussian beam. Hence we use a monopole probe with a corner reflector to produce the narrow beam in our experiments, as demonstrated in figures 3(c)–(f). Compared to the Gaussian beam, the produced beam is divergent while propagating. Similar to figures 3(a) and (b), we measure two cases where the electromagnetic waves are incident vertically and obliquely to the omnidirectional absorber. As a comparison, the full-wave numerical simulations are also given

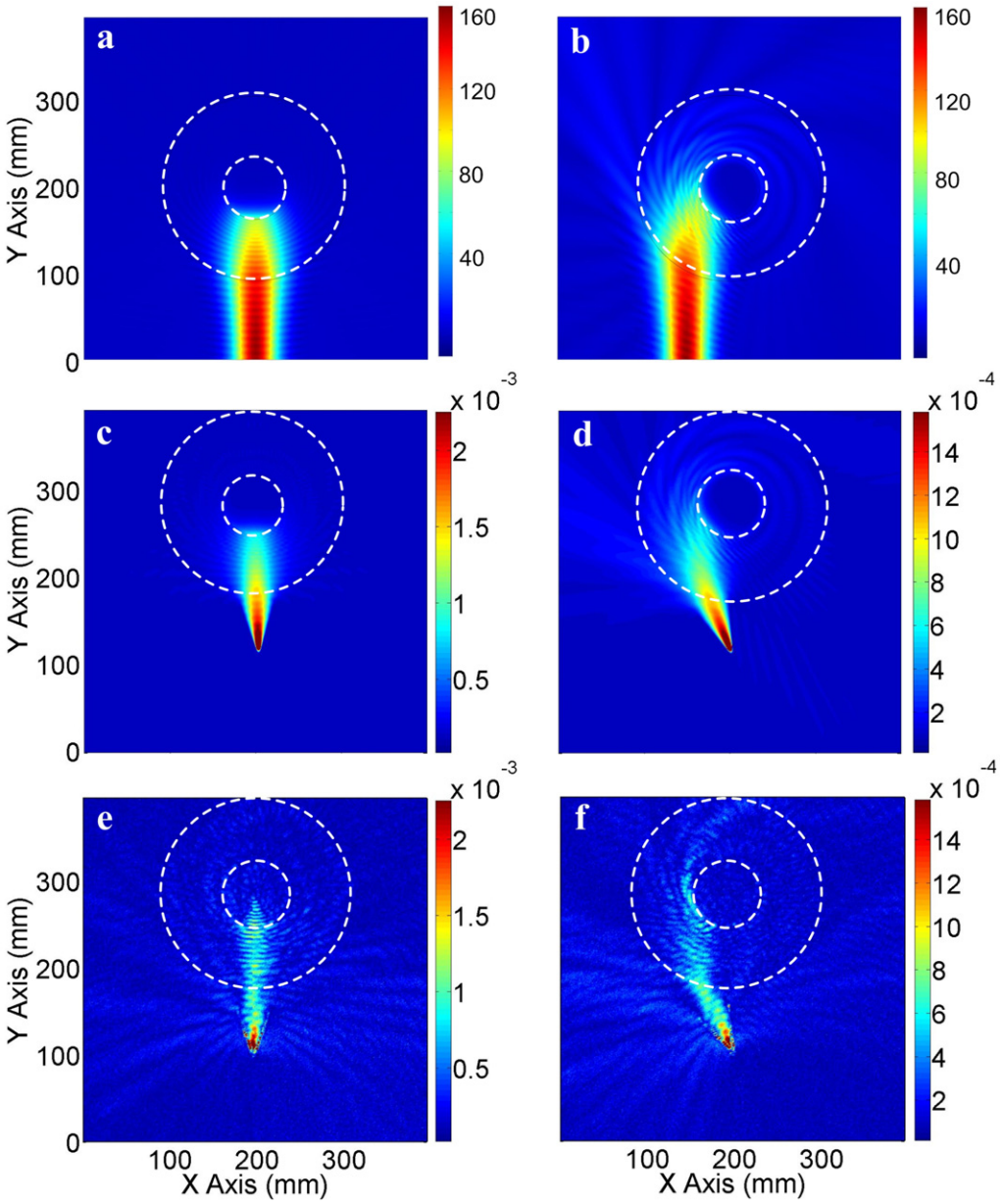

Figure 3. Distributions of electric fields $|E_z|$ for the designed omnidirectional absorbing device at the frequency of 18 GHz. An electric monopole is placed inside a corner reflector to produce the desired incident beam with finite width. The two circles stand for boundaries of the outer shell and the inner core. (a) The full-wave simulation result under the on-center incidence of a Gaussian beam. (b) The full-wave simulation result under the off-center incidence of a Gaussian beam. (c) The full-wave simulation result under the vertical incidence of the produced narrow beam. (d) The full-wave simulation result under the oblique incidence of the produced narrow beam. (e) The experimental result under the vertical incidence of the produced narrow beam. (f) The experimental result under the oblique incidence of the produced narrow beam.

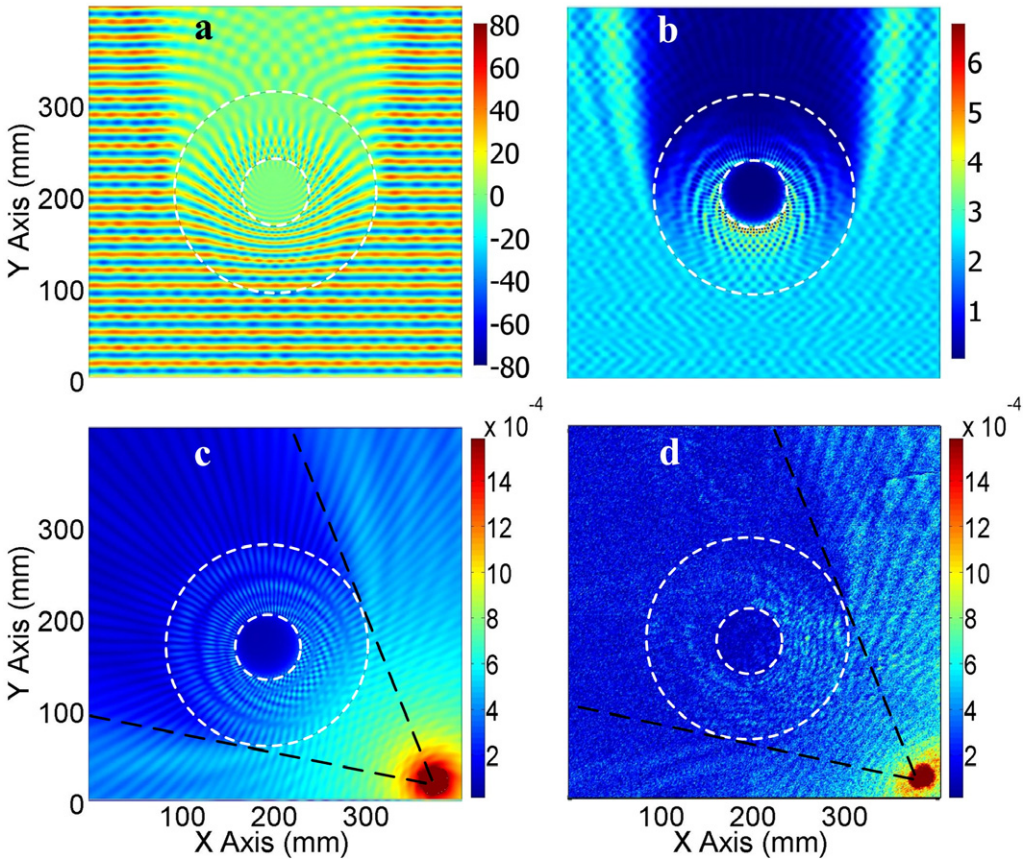

Figure 4. (a) Distributions of electric fields for the omnidirectional absorbing device at 18 GHz when a plane wave is incident. (b) Distributions of power flows for the omnidirectional absorbing device at 18 GHz when a plane wave is incident. (c) Full-wave simulation results of electric fields under the excitation of a monopole at 18 GHz. (d) Experimental results of electric fields under the excitation of the monopole at 18 GHz.

to illustrate the absorption effect. Figures 3(c) and (e) illustrate the distributions of simulated and measured electric fields $|E_z|$ at 18 GHz for the vertical-incidence case, which agree with one other very well. It is clear that the incident beam becomes convergent inside the shell region and then enters the lossy core of the device, instead of being divergent in the free-space radiation. The absorbing rate corresponding to figure 3(c) is 99.55%; nearly full absorption. When the beam is incident to the device at an oblique angle of 25°, the waves are bent toward the central area and travel around the shell spirally with distinct absorption, as shown in figures 3(d) and (f). Again, the simulation and experimental results agree well. From figure 3 we see that the device is a good attractor and absorber of microwaves.

Hence we realize the electromagnetic omnidirectional absorber experimentally in the microwave frequency, which could be used to collect microwaves and energies in free space. When the incident waves are not narrow beams, they can also be absorbed efficiently by the proposed device. Figures 4(a) and (b) demonstrate the field and power distributions inside and outside the absorbing device under the incidence of plane waves. Obviously, nearly all incident

waves hitting the device are trapped at the center and do not emerge, with an absorption rate of 99.12%. Being absorbed by the device, the incident waves hitting it cannot go through, and the total fields are nearly zero in the front region, making a complete shadow. We also note that the omnidirectional absorbing device almost does not disturb the electromagnetic waves in other regions. When the incident waves are excited by a nearby monopole, the simulated and measured field distributions are shown in figures 4(c) and (d), respectively. As with the case of plane-wave incidence, nearly all incident waves hitting the absorber (see the black dashed lines) are absorbed, producing a shadow region. The simulated and measured results agree well.

4. Summary

In summary, we have designed, fabricated and measured an electromagnetic omnidirectional absorbing device at the microwave frequency using non-resonant I-shaped metamaterials and resonant ELC metamaterials based on theoretical study [16]. We observed that nearly all incident waves and energies hitting the designed device from every direction are attracted and absorbed. Hence the device behaves like an 'electromagnetic black body' or 'electromagnetic black hole' to some extent. The good agreement between theoretical and experimental results has shown the excellent capability of metamaterials as a candidate for construction of artificial omnidirectional absorbing devices. Since the lossy core can transfer electromagnetic energies into heat energies, we expect that the proposed device could find important applications in thermal emitting and electromagnetic-wave harvesting.

Acknowledgments

This work was supported in part by the National Science Foundation of China under grant nos. 60990320, 60990324, 60871016, 60496317 and 60901011, in part by the Natural Science Foundation of Jiangsu Province under grant no. BK2008031, in part by the 111 Project under grant no. 111-2-05, and in part by the National Doctoral Foundation of China under grant no. 20090092120014.

References

[1] Smith D R, Padilla W J, Vier D C, Nemat-Nasser S C and Schultz S 2000 *Phys. Rev. Lett.* **84** 4184
[2] Smith D R, Pendry J B and Wiltshire M C K 2004 *Science* **305** 788
[3] Zhang X and Liu Z W 2008 *Nat. Mater.* **7** 435
[4] Soukoulis C M, Linden S and Wegener M 2007 *Science* **315** 47
[5] Schurig D *et al* 2006 *Science* **314** 977
[6] Leonhardt U 2006 *Science* **312** 1777
[7] Liu R, Ji C, Mock J J, Chin J Y, Cui T J and Smith D R 2009 *Science* **323** 366
[8] Valentine J, Li J, Zentgraf T, Bartal G and Zhang X 2009 *Nat. Mater.* **8** 568
[9] Cai W S, Chettiar U K, Kildishev A V and Shalaev V M 2007 *Nat. Photonics* **1** 224
[10] Leonhardt U and Tyc T 2009 *Science* **323** 110
[11] Greenleaf A, Kurylev Y, Lassas M and Uhlmann G 2007 *Phys. Rev. Lett.* **99** 183901
[12] Ma G M, Ong C K, Tyc T and Leonhardt U 2009 *Nat. Mater.* **8** 639
[13] Jiang W X, Cui T J, Cheng Q, Chin J Y, Yang X M, Liu R and Smith D R 2008 *Appl. Phys. Lett.* **92** 264101
[14] Schurig D, Mock J J and Smith D R 2006 *Appl. Phys. Lett.* **88** 041109

[15] Tsakmakidis K L, Boardman A D and Hess A 2007 *Nature* **450** 397
[16] Narimanov E E and Kildishev A V 2009 *Appl. Phys. Lett.* **95** 041106
[17] Genov D A, Zhang S and Zhang X 2009 *Nat. Phys.* **5** 687
[18] Landau L D and Lifshitz E M 1999 *The Classical Theory of Fields,* 4th edn (Portsmouth, NH: Heinemann)
[19] Smith D R, Schultz S, Markos P and Soukoulis C M 2002 *Phys. Rev.* B **65** 195104
[20] Justice B J *et al* 2006 *Opt. Express* **14** 8694